crystals

MDPI

Article

Enhanced Thermoelectric Performance of Te-Doped $Bi_2Se_{3-x}Te_x$ Bulks by Self-Propagating High-Temperature Synthesis

Rui Liu, Xing Tan, Guangkun Ren, Yaochun Liu, Zhifang Zhou, Chan Liu, Yuanhua Lin * and Cewen Nan

State Key Laboratory of New Ceramics and Fine Processing, Tsinghua University, Beijing 100084, China; liur15@mails.tsinghua.edu.cn (R.L.); tanx14@mails.tsinghua.edu.cn (X.T.); rgk13@mails.tsinghua.edu.cn (G.R.); liuyaoch@126.com (Y.L.); zhifangzhou@163.com (Z.Z.); liuchan16@mails.tsinghua.edu.cn (C.L.); cwnan@mail.tsinghua.edu.cn (C.N.)

* Correspondence: linyh@mail.tsinghua.edu.cn; Tel.: +86-10-6277-3741

Academic Editor: George S. Nolas

Received: 12 June 2017; Accepted: 21 August 2017; Published: 28 August 2017

Abstract: Polycrystalline $Bi_2Se_{3-x}Te_x$ (x = 0~1.5) samples were prepared by self-propagating high-temperature synthesis (SHS) combined with spark plasma sintering (SPS) and their thermoelectric properties were investigated. The SHS-SPS process can shorten the time with few energy consumptions, and obtain almost pure Bi_2Se_3-based phases. Consequently, the Se vacancies and anti-site defects contribute to the converged carrier concentration of ~2×10^{19} cm^{-3} while the increased carrier effective mass enhances the Seebeck coefficient to more than -158 μV K^{-1} over the entire temperature range. The lattice thermal conductivity is suppressed from 1.07 Wm^{-1} K^{-1} for the pristine specimen to ~0.6 Wm^{-1} K^{-1} for Te-substitution samples at 300 K because of point defects caused by the difference of mass and size between Te and Se atoms. Coupled with the enhanced power factor and reduced lattice thermal conductivity, a high ZT of 0.67 can be obtained at 473 K for the $Bi_2Se_{1.5}Te_{1.5}$ sample. Our results reveal that Te-substitution based on the SHS-SPS method is highly-efficient and can improve the thermoelectric properties of Bi_2Se_3-based materials largely.

Keywords: $Bi_2Se_{3-x}Te_x$; thermoelectric; SHS; solid solution

1. Introduction

With increasing attention on the environmental protection and renewable resources, thermoelectric (TE) instruments, which can directly convert heat into electricity, are considered as a potential solution for harness waste heat [1–3]. Considerable numbers of efforts have been devoted to improving the energy conversion efficiency and the stability of the TE materials [4]. The conversion efficiency depends positively on the dimensionless figure of merit, $ZT = S^2\sigma T/\kappa$, where S is the Seebeck coefficient, σ is the electrical conductivity, κ is the thermal conductivity and T is the absolute temperature, respectively [5]. To maximize the ZT value of a kind of material, a large Seebeck coefficient, electrical conductivity and low thermal conductivity are needed. However, these parameters have a strong coupling with each other, which makes it a challenging task to enhance ZT significantly. Motivated by achieving high thermoelectric performance, multiple methods have been adopted [6]. Many studies so far have focused on the atomic or molecular scales such as doping or alloying to enhance carrier concentration or carrier mobility and thus electrical conductivity to optimize TE performance [7–10]. To enhance Seebeck coefficient while maintaining high electrical conductivity, manipulating the band structure offers a new guideline [11]. Meanwhile, effective alteration at nanometer or mesoscopic scales including the quantum confinement [12] and energy filtering effect [13] can drastically elevate electrical properties.

And developing multi-scale microstructures can obtain a lower thermal conductivity, which is caused by the phonons scattering from high to low frequencies [14]. Besides, further efforts have been made to explore new TE materials and new synthesis methods [15–17].

Bismuth selenide (Bi_2Se_3) is a V-VI semiconductor with a narrow band gap of ~0.3 eV. Several excellent work describing its application of optical recording system [18] and photoelectrochemical devices [19] can be found elsewhere. Because of good TE properties in the mid-temperature, bismuth chalcogenides gained more attention [20–23] in thermoelectrics. Bi_2Se_3 has a rhombohedral layered structure, where Se-Se layers are bonded by van der Waals [24]. On the basis of the weak inter-layer bonding, Sun et al. have reported on the enhancement of the thermoelectric properties of Bi_2Se_3 by the interlayer Cu doping [22]. So far, Bi-Te-Se crystals could be fabricated through the zone melting method [25]. Bi_2Se_3 nanostructures have been synthesized by solvothermal method and *ZT* of 0.096 was obtained at 523 K [26]. Similarly, for $Bi_2Se_{3-x}Te_x$ ($x \leq 1.5$), Liu prepared by ball milling, but only achieved *ZT* of ~0.3 [9]. Nonetheless, the mentioned methods of zone melting, solvothermal method and ball milling et al. are time and energy consuming. Meanwhile, the *ZT* of Bi_2Se_3-based materials is not large enough to meet the requirements of application in mass production. In contrast, self-propagating high-temperature synthesis (SHS) has been proved to be an efficient method to prepare the TE materials alternatively. When the heating rate and temperature are high enough, the reaction wave appears. The heat generated by the exothermic reaction can maintain the whole combustion process, which is exceptionally fast. It shortens the time with few consumptions and can be easily adopted in the commercial application [27]. A wide range of TE materials have been synthesized successfully by this method, including Cu_2Se, BiCuSeO, Cu_3SbSe_3 and so on [27–30].

Previous work showed that Bi_2Se_3 and Bi_2Te_3 can be prepared by SHS method [31]. However, there are few studies focusing on the thermoelectric properties of $Bi_2Se_{3-x}Te_x$ ($x \leq 1.5$) prepared by combustion method. In this work, we successfully synthesized $Bi_2Se_{3-x}Te_x$ (x = 0, 0.3, 0.6, 0.9, 1.2, 1.5) via the SHS method followed by spark plasma sintering (SPS) and studied the thermoelectric properties from 300 K to 593 K. Our results show that the highest power factor ($PF = S^2\sigma$) can achieve 11.2 μWcm^{-1} K^{-2} for $Bi_2Se_{1.5}Te_{1.5}$ at 300 K and the lattice thermal conductivity (κ_L) could be reduced to the lowest value of 0.35 Wm^{-1} K^{-1} at 593 K via Te alloying for $Bi_2Se_{2.1}Te_{0.9}$. The *ZT* of ~0.67 is finally achieved at 473 K for $Bi_2Se_{1.5}Te_{1.5}$, demonstrating the potential application for energy conversion in the mid-temperature. And SHS process will have more hopeful prospects in commercial applications.

2. Experimental Procedures

In the initial stage, Bi (99.99%, Aladdin), Se (99.99%, Aladdin), and Te (99.99%, Aladdin) powders were mixed meticulously in stoichiometric amounts. Then the mixture was cold-pressed into pellets with the diameter of 20 mm. The SHS process was started by heating the bottom of the pellets with a hand torch in the air. Once ignited, the hand torch is removed immediately. The heat generated by the combination reaction kept the combustion process propagating until it was finished in several seconds. Then the pellets were grounded into fine powders carefully by hand. The powders were then sintered into pellets of ϕ 12.7 mm by SPS (Sumitomo Coal Mining Co., Ltd., Tokyo, Japan) at the temperature of 593 K for 5 min under a uniaxial pressure of 40 MPa.

The phase structures were investigated by X-ray diffraction (XRD, RINT2000, Rigaku, Tokyo, Japan) analysis. The morphology and composition of cross-sectional bulks were checked by field-emission scanning electron microscopy (FESEM) (LEO1530, Oxford Instruments, Oxford, UK). The electrical properties including electrical conductivity and Seebeck coefficient were measured from room temperature to 593 K by ZEM-3 (ULVAC, Kanagawa, Japan). The van der Pauw method was used in an Eastchanging Hall measurement station to measure Hall coefficient (R_H). The carrier concentration (n) and mobility (μ) were estimated by the equation $n = 1/eR_H$ and $\mu = \sigma R_H$. To ensure the accuracy, the samples were polished to be thinner than 0.5 mm for the measurements. The total thermal conductivity is determined by the equation $\kappa = DC_p\rho$, where D is thermal diffusivity, C_p is specific heat and ρ is the density of the bulks. The thermal diffusivity was obtained by the laser flash

method and the specific heat was calculated by the Dulong-Petit relation. The density of the bulks was derived with Archimedes method.

3. Results and Discussion

Figure 1a is the XRD result of all the $Bi_2Se_{3-x}Te_x$ samples with x = 0~1.5. All the major peaks in the XRD patterns correspond to a standard card, Bi_2Se_3, PDF #33-0214. The additional small peaks can be identified as Bi_2O_2Se (PDF #29-0237), which is possibly generated by oxidation during the ultra-fast combustion process in the air. In this work, we assume that all the samples contain the same amount of Bi_2O_2Se, and we neglect the effect of existence of Bi_2O_2Se due to its small amount (small peaks in the XRD result). In Figure 1b, the lattice parameters were calculated according to the position of XRD peaks. With increasing Te content, the lattice constants a and c increase linearly, which indicates Te can successfully substitute for Se atoms to form solid solution by SHS process in a short time. Figure 1c–e show the morphology of cross-sectional bulks (x = 0, 0.3, 1.5). All the samples were sintered well with high density (94% or above). The layer structure can be seen clearly in the $Bi_2Se_{3-x}Te_x$ bulks.

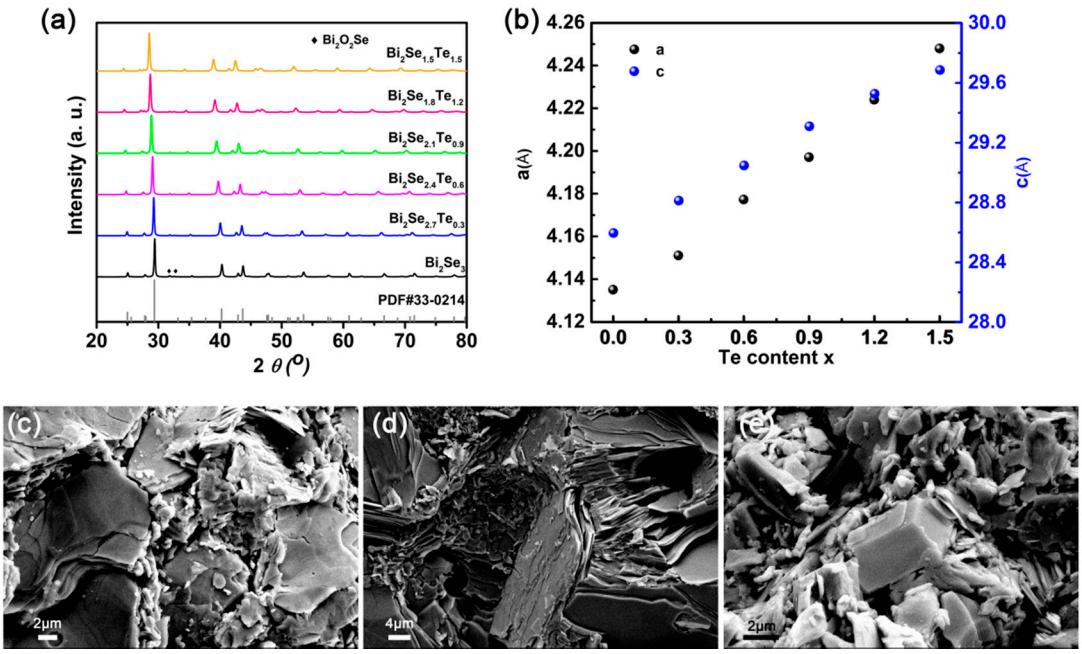

Figure 1. (**a**) XRD patterns and (**b**) lattice parameters of sintered $Bi_2Se_{3-x}Te_x$ bulk samples; field-emission scanning electron micrographs of $Bi_2Se_{3-x}Te_x$, for which, (**c**) x = 0; (**d**) x = 0.3; and (**e**) x = 1.5.

Figure 2 shows the temperature dependence of electrical conductivity and Seebeck coefficient. The electrical conductivity σ (in Figure 2a) of pristine Bi_2Se_3 maintains at about 400 Scm^{-1} from 300 K to 593 K, which is much higher than Bi_2Se_3 prepared by other method [22]. Se is much easier to evaporate during the combustion process because of low energy of evaporation and thus it leaves Se vacancies and free electrons, which may contribute to higher electrical conductivity. This can be indicated in the following equation:

$$Bi_2Se_3 = 2Bi_{Bi}^{\times} + (3-y)Se_{Se}^{\times} + ySe(g)\uparrow + yV_{Se}^{2+} + 2ye^- \quad (1)$$

As the Te content increases (x > 0), the electrical conductivity at 300 K initially increases to ~870 Scm^{-1} because of increased carrier concentration (Table 1), then decreases to ~400 Scm^{-1} owing to the change of carrier mobility, which is much lower than the pristine Bi_2Se_3 (Table 1). The carrier concentration increases

may be a result of increasing anti-site defects (Bi_{Te}^{-}) [31], which is caused by the fact that Bi can jump from Bi-site to Te-site easily because of small difference in electronegativity [10], as indicated in Equation (2).

$$Bi_2Te_3 = (2 - \frac{2}{5}z)Bi_{Bi}^{\times} + (3 - z)Te_{Te}^{\times} + zTe(g) \uparrow + (\frac{2}{5}zV_{Bi}^{3-} + \frac{3}{5}zV_{Te}^{2+}) + \frac{2}{5}zBi_{Te}^{-} + \frac{2}{5}zh^{+} \quad (2)$$

On the contrary, the number of Se vacancies V_{Se}^{2+} will be fewer due to the increasing Te content. The decreased Se vacancies and increased anti-site defects make the carrier concentration converges to about 2×10^{19} cm^{-3}. The carrier mobility decreases with higher Te content at 300 K in general due to the enhanced alloy scattering. Interestingly, we found μ of $Bi_2Se_{1.5}Te_{1.5}$ (x = 1.5) is slightly larger than $Bi_2Se_{1.8}Te_{1.2}$ (x = 1.2) at the room temperature, which is possibly caused by the intrinsic high mobility of Bi_2Te_3 [31].

Table 1. Actual composition, carrier concentration (n), carrier mobility (μ), carrier effective mass (m^*), Seebeck coefficient (S), Lorenz constant (L), lattice thermal conductivity (κ_L), κ_L/κ, and density of $Bi_2Se_{3-x}Te_x$ samples at 300 K.

x	n (10^{18} cm^{-3})	μ (cm^2 V^{-1} s^{-1})	m^*/m_0	S (μV K^{-1})	L (10^{-8} V^2 K^{-2})	κ_L (Wm^{-1} K^{-1})	κ_L/κ	Density (g cm^{-3})
0.0	5.94	444.48	0.19	−118.23	1.83	1.07	81.7%	7.01
0.3	17.31	309.19	0.25	−73.65	2.06	0.80	59.4%	6.92
0.6	21.94	209.36	0.31	−79.95	2.03	0.62	57.4%	6.77
0.9	24.42	149.33	0.45	−107.68	1.88	0.52	60.4%	6.65
1.2	24.37	97.45	0.53	−126.49	1.81	0.60	74.0%	6.83
1.5	20.73	134.96	0.60	−158.72	1.71	0.59	71.6%	6.96

As shown in Figure 2b, the negative Seebeck coefficient of all the samples indicates the dominance of electrons in the transport process. Generally, the value of Seebeck coefficient can be estimated by the equation [32]:

$$|S| = \frac{8\pi^2 k_B^2 T}{3eh^2} m_d^* (\frac{\pi}{3n})^{2/3} \quad (3)$$

where e, k_B, T, h, m_d^*, and n are the carrier charge, Boltzmann constant, absolute temperature, Planck constant, the effective mass of the carrier, and carrier concentration. As shown in the formula, because of largely enhanced carrier concentration with increasing Te content (x < 0.9) at 300 K, the Seebeck coefficient decreases. Then the Seebeck coefficient was improved due to the larger carrier effective mass at 300 K (Table 1). It should be noticed that each sample with x $\geq$ 0.9, as the temperature increases, the value of Seebeck coefficient first increases then decreases, which is caused by the intrinsic excitations. The highest Seebeck coefficient of −180 μV K^{-1} is achieved at 473 K for the $Bi_2Se_{1.5}Te_{1.5}$ sample. The $Bi_2Se_{1.5}Te_{1.5}$ sample attains the largest effective mass of ~0.60 m_0, which is in accord with the difference of Seebeck coefficient with different Te contents at room temperature.

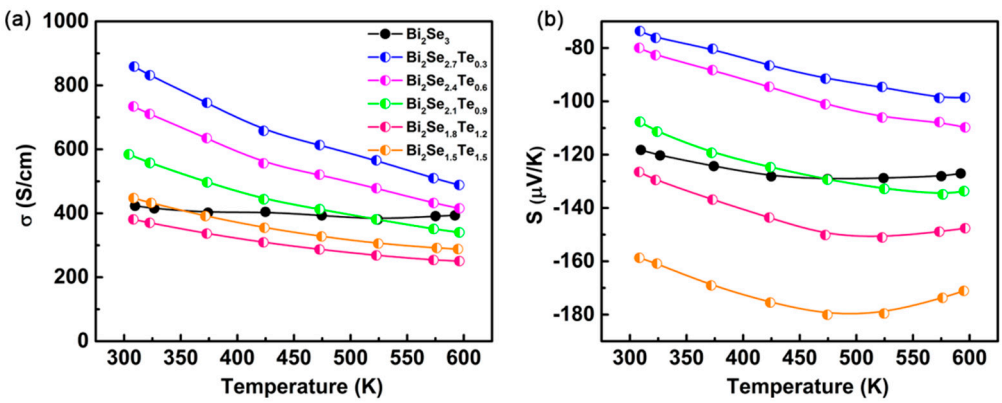

Figure 2. Temperature dependence of (**a**) electrical conductivity and (**b**) Seebeck coefficient for $Bi_2Se_{3-x}Te_x$ samples.

The variation of power factor ($PF = S^2\sigma$) with increasing temperature of all the samples is shown in Figure 3. The $Bi_2Se_{1.5}Te_{1.5}$ sample reaches the highest *PF* of 11.2 μWcm^{-1} K^{-2} at room temperature, which is almost twice higher than that of pristine Bi_2Se_3. But it drops to about 8 μWcm^{-1} K^{-2} at 593 K owing to the decreased electrical conductivity and Seebeck coefficient.

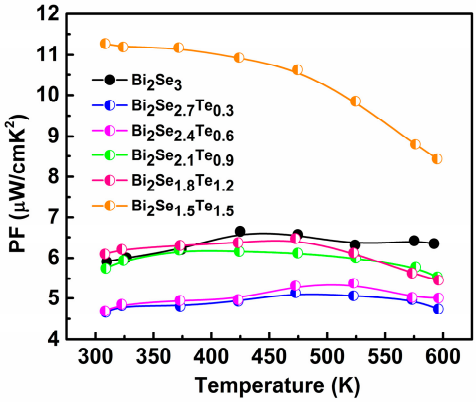

Figure 3. The temperature dependence of power factor for $Bi_2Se_{3-x}Te_x$ samples.

Figure 4a illustrates the total thermal conductivity (κ) as a function of temperature from room temperature to 593 K. The κ of pristine Bi_2Se_3 is in the range of 1.04–1.31 Wm^{-1} K^{-1}. As x increases to 1.2, the κ drops into the range of 0.76–0.82 Wm^{-1} K^{-1} from 300 K to 593 K. With further increasing Te content, κ is much larger than the sample of x = 1.2. To have a better understanding of the thermal transport properties, κ is subsequently divided into three parts:

$$\kappa = \kappa_e + \kappa_L + \kappa_B \tag{4}$$

where κ_e is electron thermal conductivity, κ_L is lattice thermal conductivity and κ_B is the bipolar thermal conductivity induced by intrinsic excitaions. κ_e can be estimated by Wiedemann-Franz relation:

$$\kappa_e = L\sigma T \tag{5}$$

where L is the Lorenz constant and σ is electrical conductivity. In the single parabolic band model, L depends on the reduced chemical potential and scattering parameter. It can be estimated by fitting the values of the Seebeck coefficient and the room temperature data has been listed in Table 1. The details can be seen elsewhere [33,34]. As mentioned above (Figure 2b), intrinsic excitaions don't occur until 423 K or above. Therefore, the κ_B can be ignored at low temperature in Figure 4b. Consequently, κ_L and the reciprocal temperature, T^{-1}, follow a linear relationship. As shown in Figure 4c, the lattice thermal conductivity drops substantially after alloying. Note that the κ_L of $Bi_2Se_{2.1}Te_{0.9}$ achieves the lowest value of 0.35 Wm^{-1} K^{-1} at 593 K. The effective suppression of the κ_L of could be attributed to point defects caused by the different mass and size between Te and Se atoms. Similar to the previous literature [9], the κ_L rises slightly when x is above 0.9. This may be ascribed to the relatively high κ_L of Bi_2Te_3 [31], whose effect is larger than the point defects. Figure 4d shows the temperature dependence of κ_B. With low Te content ($x \leq 0.6$), κ_B is almost zero from 300 K to 593 K, because there are no intrinsic excitaions. Intrinsic excitaions occur and κ_B's contribution to κ becomes larger when $x \geq 0.9$, which is owing to narrower band gap with increasing Te content [35].

The *ZT* values for all the $Bi_2Se_{3-x}Te_x$ samples (x = 0, 0.3, 0.6, 0.9, 1.2, 1.5) are presented in Figure 5. The enhanced power factor and the effective suppression of lattice thermal conductivity synergistically contribute to the highest *ZT* value of 0.67 at 473 K for the sample of $Bi_2Se_{1.5}Te_{1.5}$, which is almost twice higher than the pristine Bi_2Se_3. *ZT* values of Bi_2Se_3 (ball milling) [22], Bi_2Se_2Te (ball milling) [9],

Bi_2Te_3 (SHS) [31] from the literature are included for comparison. Our results show that the *ZT* value of Te-substituted Bi_2Se_3-based materials prepared by SHS is much larger than that by other methods.

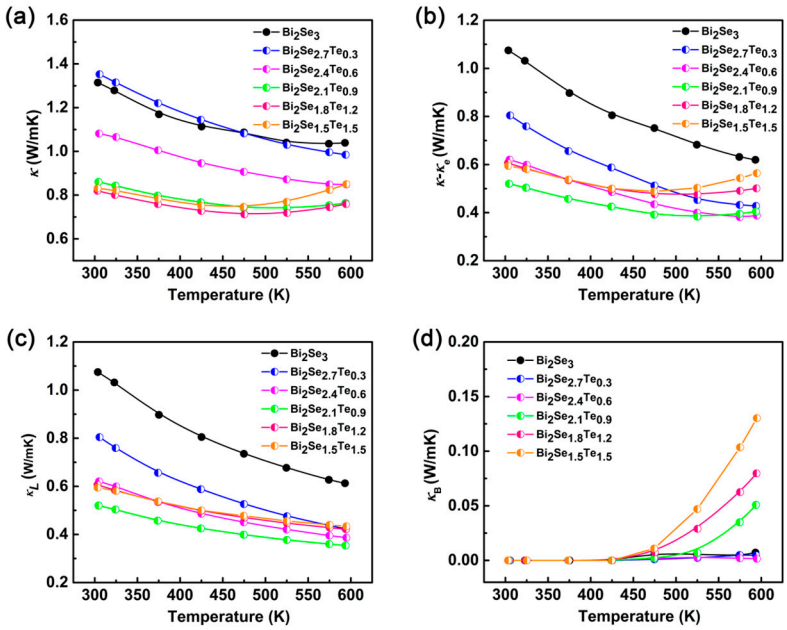

Figure 4. The temperature dependence of the (**a**) total thermal conductivity; (**b**) $\kappa - \kappa_B$; (**c**) lattice thermal conductivity; and (**d**) the bipolar thermal conductivity for $Bi_2Se_{3-x}Te_x$ samples.

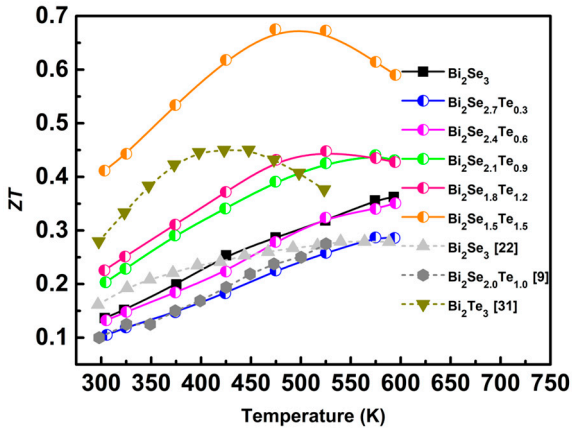

Figure 5. The temperature dependence of ZT for $Bi_2Se_{3-x}Te_x$ samples.

4. Conclusions

In summary, we have investigated the thermoelectric properties (300–593 K) of $Bi_2Se_{3-x}Te_x$ samples (x = 0, 0.3, 0.6, 0.9, 1.2, 1.5), which are prepared by SHS-SPS process successfully. Compared with other methods, the SHS-SPS process is much faster and requires less energy, which is desirable in commercial application even though with small amount of second phase Bi_2O_2Se. Our results show that the power factor of $Bi_2Se_{1.5}Te_{1.5}$ achieves 11.2 μWcm^{-1} K^{-2} at 300 K by the increased carrier concentration and the enhancement of Seebeck coefficient. The point defects originate from the difference of mass and size between Te and Se atoms significantly suppresses the lattice thermal conductivity. Benefiting from the improved power factor and the decreased lattice thermal conductivity, a high *ZT* of 0.67 can be obtained at 473 K for the sample of $Bi_2Se_{1.5}Te_{1.5}$, which demonstrates that the Te-substitution via SHS-SPS method is highly-efficient and can enhance the thermoelectric properties of Bi_2Se_3-based materials.

Acknowledgments: This work was supported by the National Key Research Programme of China, under grant No. 2016YFA0201003, Ministry of Sci & Tech of China through a 973-Project under grant No. 2013CB632506, and National Science Foundation of China under grand No. 51672155 and 51532003.

Author Contributions: Rui Liu performed the experiments and wrote the paper. Guangkun Ren, Yaochu Liu, Cewen Nan and Yuanhua Lin revised the manuscript. Chan Liu, Xing Tan and Zhifang Zhou assisted in experiments.

Conflicts of Interest: The authors declare no conflict of interest.

References

1. Yang, S.H.; Zhu, T.J.; Sun, T.; He, J.; Zhang, S.N.; Zhao, X.B. Nanostructures in high-performance $(GeTe)_x(AgSbTe_2)_{100-x}$ thermoelectric materials. *Nanotechnology* **2008**, *19*, 245707. [CrossRef] [PubMed]
2. Bell, L.E. Cooling, heating, generating power, and recovering waste heat with thermoelectric systems. *Science* **2008**, *321*, 1457–1461. [CrossRef] [PubMed]
3. Tritt, T.M. Holey and unholey semiconductors. *Science* **1999**, *283*, 804. [CrossRef]
4. Rhyee, J.S.; Lee, K.H.; Lee, S.M.; Cho, E.; Kim, S.I.; Lee, E.; Kwon, Y.S.; Shim, J.H.; Kotliar, G. Peierls distortion as a route to high thermoelectric performance in $In_4Se_{3-\delta}$ crystals. *Nature* **2009**, *459*, 965–968. [CrossRef] [PubMed]
5. Nolas, G.S.; Sharp, J.; Goldsmid, J. *Thermoelectrics: Basic Principles and New Materials Developments*; Springer: Berlin, Germany, 2013; Volume 45, p. 111.
6. Snyder, G.J.; Toberer, E.S. Complex thermoelectric materials. *Nat. Mater.* **2008**, *7*, 105–114. [CrossRef] [PubMed]
7. Mehta, R.J.; Zhang, Y.; Karthik, C.; Singh, B.; Siegel, R.W.; Borca-Tasciuc, T.; Ramanath, G. A new class of doped nanobulk high-figure-of-merit thermoelectrics by scalable bottom-up assembly. *Nat. Mater.* **2012**, *11*, 233–240. [CrossRef] [PubMed]
8. Tan, X.; Lan, J.L.; Ren, G.K.; Liu, Y.; Lin, Y.H.; Nan, C.W. Enhanced thermoelectric performance of n-type Bi_2O_2Se by Cl-doping at Se site. *J. Am. Ceram. Soc.* **2017**, *100*, 1494–1501. [CrossRef]
9. Liu, W.S.; Lukas, K.C.; McEnaney, K.; Lee, S.; Zhang, Q.; Opeil, C.P.; Chen, G.; Ren, Z.F. Studies on the Bi_2Te_3-Bi_2Se_3-Bi_2S_3 system for mid-temperature thermoelectric energy conversion. *Energy Environ. Sci.* **2013**, *6*, 552–560. [CrossRef]
10. Liu, W.S.; Zhang, Q.Y.; Lan, Y.C.; Chen, S.; Yan, X.; Zhang, Q.; Wang, H.; Wang, D.Z.; Chen, G.; Ren, Z.F. Thermoelectric property studies on Cu-doped n-type $Cu_xBi_2Te_{2.7}Se_{0.3}$ nanocomposites. *Adv. Energy Mater.* **2011**, *1*, 577–587. [CrossRef]
11. Pei, Y.Z.; Shi, X.Y.; Lalonde, A.; Wang, H.; Chen, L.D.; Snyder, G.J. Convergence of electronic bands for high performance bulk thermoelectrics. *Nature* **2011**, *473*, 66–69. [CrossRef] [PubMed]
12. Hicks, L.D.; Dresselhaus, M.S. Thermoelectric figure of merit of a one-dimensional conductor. *Phys. Rev. B* **1992**, *47*, 16631. [CrossRef]
13. Humphrey, T.E.; Linke, H. Reversible Thermoelectric Nanomaterials. *Phys. Rev. Lett.* **2005**, *94*, 096601. [CrossRef] [PubMed]
14. Biswa, K.; He, J.Q.; Blum, I.D.; Wu, C.I.; Hogan, T.P.; Seidman, D.D.; Dravid, V.P.; Kanatzidis, M.G. High-performance bulk thermoelectrics with all-scale hierarchical architectures. *Nature* **2012**, *489*, 414–418. [CrossRef] [PubMed]
15. Dresselhaus, M.S.; Chen, G.; Tang, M.Y.; Yang, R.; Lee, H.; Wang, D.; Ren, Z.; Fleurial, J.P.; Gogna, P. New directions for low-dimensional thermoelectric materials. *Adv. Mater.* **2007**, *19*, 1043–1053. [CrossRef]
16. Chen, G.; Dresselhaus, M.; Dresselhaus, G.; Fleurial, J.P.; Caillat, T. Recent developments in thermoelectric materials. *Int. Mater. Rev.* **2003**, *48*, 45–66. [CrossRef]
17. Kauzlarich, S.M.; Brown, S.R.; Snyder, G.J. Zintl phases for thermoelectric devices. *Dalton Trans.* **2007**, *21*, 2099–2107. [CrossRef] [PubMed]
18. Watanabe, K.; Sato, N.; Miyaoko, S. New optical recording material for video disc system. *J. Appl. Phys.* **1983**, *54*, 1256. [CrossRef]
19. Waters, J.; Crouch, D.; Raftery, J.; O'Brien, P. Deposition of bismuth chalcogenide thin films using novel single-source precursors by metal-organic chemical vapor deposition. *Chem. Mater.* **2004**, *16*, 3289–3298. [CrossRef]

20. Bayaz, A.A.; Giani, A.; Foucaran, A.; Pascal-Delannoy, F.; Boyer, A. Electrical and thermoelectrical properties of Bi_2Se_3 grown by metal organic chemical vapour deposition technique. *Thin Solid Films* **2003**, *441*, 1–5. [CrossRef]
21. Tang, Z.L.; Hu, L.P.; Zhu, T.J.; Liu, X.H.; Zhao, X.B. High performance n-type bismuth telluride based alloys for mid-temperature power generation. *J. Mater. Chem. C* **2015**, *3*, 10597–10603. [CrossRef]
22. Sun, G.L.; Qin, X.Y.; Li, D.; Zhang, J.; Ren, B.J.; Zou, T.H.; Xin, H.X.; Paschen, S.B.; Yan, X.L. Enhanced thermoelectric performance of n-type Bi_2Se_3 doped with Cu. *J. Alloys Compd.* **2015**, *639*, 9–14. [CrossRef]
23. Kim, D.; Syers, P.; Butch, N.P.; Paglione, J.; Fuhrer, M.S. Ambipolar surface state thermoelectric power of topological insulator Bi_2Se_3. *Nano Lett.* **2014**, *14*, 1701–1706. [CrossRef] [PubMed]
24. Nakajima, S. The crystal structure of $Bi_2Te_{3-x}Se_x$. *J. Phys. Chem. Solids* **1963**, *24*, 479–485. [CrossRef]
25. Jiang, J.; Chen, L.D.; Yao, Q.; Bai, S.Q.; Wang, Q. Effect of TeI4 content on the thermoelectric properties of n-type Bi–Te–Se crystals prepared by zone melting. *Mater. Chem. Phys.* **2005**, *92*, 39–42. [CrossRef]
26. Kadel, K.; Kumari, L.; Li, W.Z.; Huang, Y.Y.; Provencio, P.P. Synthesis and thermoelectric properties of Bi_2Se_3 nanostructures. *Nanoscale Res. Lett.* **2011**, *6*, 57. [CrossRef] [PubMed]
27. Su, X.; Fu, F.; Yan, Y.; Zheng, G.; Liang, T.; Zhang, Q.; Cheng, X.; Yang, D.; Chi, H.; Tang, X.; et al. Self-propagating high-temperature synthesis for compound thermoelectrics and new criterion for combustion processing. *Nat. Commun.* **2014**, *5*, 4908. [CrossRef] [PubMed]
28. Ren, G.K.; Lan, J.L.; Butt, S.; Ventura, K.J.; Lin, Y.H.; Nan, C.W. Enhanced thermoelectric properties in Pb-doped BiCuSeO oxyselenides prepared by ultrafast synthesis. *RSC Adv.* **2015**, *5*, 69878–69885. [CrossRef]
29. Liu, R.; Ren, G.K.; Tan, X.; Lin, Y.L.; Nan, C.W. Enhanced thermoelectric properties of Cu_3SbSe_3-based composites with inclusion phases. *Energies* **2016**, *9*, 816. [CrossRef]
30. Yang, D.W.; Su, X.L.; Yan, Y.G.; Hu, T.Z.; Xie, H.Y.; He, J.; Uher, C.; Kanatzidis, M.G.; Tang, X.F. Manipulating the combustion wave during self-Propagating synthesis for high thermoelectric performance of layered oxychalcogenide $Bi_{1-x}Pb_xCuSeO$. *Chem. Mater.* **2016**, *28*, 4628–4640. [CrossRef]
31. Zheng, G.; Su, X.L.; Liang, T.; Lu, Q.B.; Yan, Y.G.; Uher, C.; Tang, X.F. High thermoelectric performance of mechanically robust n-type $Bi_2Te_{3-x}Se_x$ prepared by combustion synthesis. *J. Mater. Chem. A* **2015**, *3*, 6603–6613. [CrossRef]
32. Koumoto, K.; Funahashi, R.; Guilmeau, E.; Miyazaki, Y.; Weidenkaff, A.; Wang, Y.F.; Wan, C.L. Thermoelectric ceramics for energy harvesting. *J. Am. Ceram. Soc.* **2013**, *96*, 1–23. [CrossRef]
33. Pei, Y.L.; He, J.; Li, J.F.; Li, F.; Liu, Q.J.; Pan, W.; Barreteau, C.; Berardan, D.; Dragoe, N.; Zhao, L.D. High thermoelectric performance of oxyselenides: Intrinsically low thermal conductivity of Ca-doped BiCuSeO. *NPG Asia Mater.* **2013**, *5*, 425–434. [CrossRef]
34. Kumar, G.S.; Prasad, G.; Pohl, R.O. Experimental determinations of the Lorenz number. *J. Mater. Sci.* **1993**, *28*, 4261–4272. [CrossRef]
35. Imamuddin, M.; Dupre, A. Thermoelectric properties of p-type Bi_2Te_3-Sb_2Te_3-Sb_2Se_3 alloys and n-type Bi_2Te_3-Bi_2Se_3 alloys in the temperature range 300 to 600 K. *Phys. Status Solidi A* **1972**, *10*, 415–424. [CrossRef]